Wind and Structures, *Vol. 29, No. 6 (2019) 457-469*
DOI: https://doi.org/10.12989/was.2019.29.6.457

Aeroelastic analysis of cantilever non-symmetric FG sandwich plates under yawed supersonic flow

Mohammad Hosseini[1], Ali Ghorbanpour Arani*[2,3], Mohammad Reza Karamizadeh[1], Hassan Afshari[4] and Shahriar Niknejad[2]

[1]*Department of Mechanical Engineering, Sirjan University of Technology, 78137-33385 Sirjan, Iran*
[2]*Faculty of Mechanical Engineering, Department of Solid Mechanics, University of Kashan, Kashan, Iran*
[3]*Institute of Nanoscience & Nanotechnology, University of Kashan, Kashan, Iran*
[4]*Department of Mechanical Engineering, Khomeinishahr Branch, Islamic Azad University, Khomeinishahr/Isfahan, Iran*

(Received April 15, 2018, Revised June 10, 2019, Accepted September 27, 2019)

Abstract. In this paper, a numerical solution is presented for supersonic flutter analysis of cantilever non-symmetric functionally graded (FG) sandwich plates. The plate is considered to be composed of two different functionally graded face sheets and an isotropic homogeneous core made of ceramic. Based on the first order shear deformation theory (FSDT) and linear piston theory, the set of governing equations and boundary conditions are derived. Dimensionless form of the governing equations and boundary conditions are derived and solved numerically using generalized differential quadrature method (GDQM) and critical velocity and flutter frequencies are calculated. For various values of the yaw angle, effect of different parameters like aspect ratio, thickness of the plate, power law indices and thickness of the core on the flutter boundaries are investigated. Numerical examples show that wings and tail fins with larger length and shorter width are more stable in supersonic flights. It is concluded for FG sandwich plates made of Al-Al_2O_3 that increase in volume fraction of ceramic (Al_2O_3) increases aeroelastic stability of the plate. Presented study confirms that improvement of aeroelastic behavior and weight of wings and tail fins of aircrafts are not consistent items. It is shown that value of the critical yaw angle depends on aspect ratio of the plate and other parameters including thickness and variation of properties have no considerable effect on it. Results of this paper can be used in design and analysis of wing and tail fin of supersonic airplanes.

Keywords: aeroelasticity; flutter; yawed flow; cantilever plate; sandwich plate

1. Introduction

In order to achieve an optimal performance of a construction, sandwich structures with different types of cores such as homogenious materials, FG materials, porous materials, honeycombs (Hatami-Marbini and Rohanifar 2019) and reological fluids (Hasheminejad *et al.* 2013) can be used. Due to the remarkable mechnaical properties of metals and high thermal performance of ceramics, FG structures and FG-sandwich structures have attained wide acceptance in aerospace and many other industries. These types of composite structures are widely employed in aircraft and space vehicles and revolutionized the aerospace industry over 40 years ago, making aircrafts lighter, stronger and faster, and allowing them to carry more weight and improve fuel efficiency (Tounsi *et al.* 2013).

Flutter phenomenon is one of the most important items need to be investigated in the design of aircrafts (Afshari and Torabi 2017a, Torabi *et al*. 2017b, Torabi *et al.* 2017) and long-span bridges (Han *et al*. 2015, Wang *et al*. 2016, Tang *et al.* 2017). Cantilever plates can be used to model many structures in mechanical, civil and aerospace engineering. As flight velocity of an aircraft rises, the self-excited vibration of wing or tail fin will occur which is known as the flutter. As flutter can be dangerous to the aircraft safety, numerous researchers have studied the flutter characteristics for structures. Srinivasan and Babu (1985) used finite element method (FEM) for flutter analysis of quadrilateral plates and presented both critical dynamic pressure and flutter frequency for various boundary conditions. A shear deformable element was used by Chowdary *et al*. (1996) to investigate the supersonic flutter of composite skew plates. For different boundary conditions and fiber orientation, they studied effect of skew angle on the critical dynamic pressure. Using FEM, Singha and Ganapathi (2005) presented a parametric study on supersonic flutter behavior of laminated composite skew plates. For different boundary conditions, they studied effect of skew angle and fiber orientation on the critical aerodynamic pressure. Prakash and Ganapathi (2006) employed FEM and investigated influence of temperature on the supersonic flutter characteristics of FG flat panels. Singha and Mandal (2008) used isoparametric finite element formulation and studied supersonic flutter analysis of laminated composite plates and cylindrical panels. They investigated effects of different parameters on the supersonic flutter characteristics including curvature, laminate stacking sequence, air flow direction and boundary condition. Using FEM and quasi-steady aerodynamic theory, Kuo (2011) studied effect of variable fiber spacing on the supersonic flutter of rectangular composite plates. He

*Corresponding author, Professor
E-mail: aghorban@kashanu.ac.ir

ISSN: 1226-6116 (Print), 1598-6225 (Online)

showed that flutter boundaries may be increased or decreased due to variable fiber spacing. Based on the FSDT for plate and local piston theory for aerodynamic pressure in supersonic flow, Meijer and Dala (2015) used a finite element structural model and developed a zeroth-order flutter prediction for cantilever plates. Sankar *et al.* (2015) used a higher-order structural theory and QUAD-8 shear flexible shell element and studied supersonic flutter behavior of doubly curved sandwich panels with carbon nanotube (CNT) reinforced face sheets. They studied effect of the volume fraction of the CNT, core-to-face sheet thickness, total thickness, aspect ratio, radius-to-thickness ratio and temperature on the flutter boundaries. Using FEM, Cunha-Filho *et al.* (2016) presented a numerical study on the flutter analysis of a three-layer sandwich rectangular plate. They studied the possibility of reducing the effects of the supersonic aeroelastic instability of plates using passive constrained viscoelastic layers.

Using Galerkin method, some authors studied flutter analysis of structures; i.e., Navazi and Haddadpour (2011) studied nonlinear aeroelastic behavior of homogeneous and functionally graded two dimensional and three-dimensional flat plates under supersonic airflow. They showed that under real flight conditions and using coupled model, the type of instability is divergence. Based on the classical Love's shell theory and the first-order piston theory for aerodynamic loading and also considering temperature-dependent properties, Haddadpour *et al*. (2008) and Mahmoudkhani *et al.* (2010) focused on supersonic aero-thermoelastic analysis of a functionally graded cylindrical and truncated conical shells, respectively. For the cylindrical shells they investigated effects of power-law index, internal pressure and temperature rise on the flutter boundaries and for the conical one they predicted the flutter boundaries for different values of semi-vertex cone angles, different temperature distributions, and different volume fraction indices. Kouchakzadeh *et al.* (2010) studied nonlinear aeroelasticity of a general laminated composite plate in supersonic airflow. They used the classical plate theory and the von-Karman nonlinear strains for structural modeling and also linear piston theory for aerodynamic modeling and studied effects of in-plane force, static pressure differential, fiber orientation and aerodynamic damping on the aeroelastic characteristics of the plate. They showed that the fiber orientation has significant effect on dynamic behavior of the plate. Vedeneev focused on the single mode flutter analysis which happens at low supersonic speeds. He presented a comprehensive numerical solution of single mode flutter (Vedeneev 2012). As he employed Euler-Bernoulli beam theory, accuracy of his results were limit to panels of high aspect ratios. In another work, he investigated effect of damping on single mode panel flutter of panels at low supersonic speeds (Vedeneev 2013). He showed that for typical structural, damping levels single mode flutter is not always avoidable. Moreover, for some conditions damping level necessary to suppress flutter is too high and cannot be achieved by the structure itself. He and his coworkers (2010) presented an experimental study on single mode flutter of panels in supersonic gas flow. Using von Karman nonlinear strain–displacement relations, Hosseini *et al.* (2011) studied nonlinear analysis of functionally graded curved panels under high temperature supersonic gas flows. They investigated effects of volume fraction index, curved panel height-rise, and aerodynamic pressure, in conjunction with the applied thermal loading, on the dynamical behavior of the panel. Hosseini and Fazelzadeh (2010) the aerothermoelastic post-critical and vibration characteristics of temperature-dependent functionally graded panels in a supersonic airflow. They investigated panel vibration responses through time history responses, state-space trajectories, frequency spectra and the bifurcation diagrams of Poincaré maps.

Using DQM, Torabi and afshari focused on vibration, supersonic flutter and aeroelastic optimization of cantilever trapezoidal moderately thick plates. They modeled the plate based on the FSDT and estimated aerodynamic pressure of external flow using the piston theory. Torabi and afshari (2016, 2017c) studied vibration analysis of cantilever trapezoidal thick plates of non-uniform thickness or uniform ones made of functionally graded materials. Afshari and Torabi (2017) presented a parametric study on flutter behavior of cantilever trapezoidal functionally graded sandwich plates. Torabi *et al.* (2017) studied vibration and supersonic flutter analysis of cantilever trapezoidal honeycomb sandwich plates. Torabi and afshari (2017a, b) used particle swarm optimization (PSO) and found the best configuration of the cantilever trapezoidal thick plates of non-uniform thickness or uniform ones made of FG face sheets and homogeneous core which leads to maximum value of the critical aerodynamic pressure. Ghorbanpour Arani *et al*. (2019a, b) used third order shear deformation theory (TSDT) and studied free vibration and flutter analysis of laminated functionally graded carbon nanotube (CNT) reinforced cylindrical panels under yawed supersonic flow. They studied effect of geometrical parameters, volume fraction and distribution of CNTs and yaw angle on the natural frequencies, critical speed and flutter frequency.

In this paper, supersonic flutter analysis of cantilever sandwich plates with non-symmetric FG face sheets is presented. The plate is modeled using the FSDT and aerodynamic pressure is estimated based on the linear piston theory for a desired yaw angle. Effect of different parameters on the variation of the critical speed versus yaw angle are investigated including aspect ratio, total thickness, relative thickness of the core and face sheets and power law indices.

2. Governing equations

As depicted in Fig. 1, a Cantilever plate clamped at y=0 and free at other edges is considered. It is assumed that the plate is exposed to a compressible supersonic flow of density ρ_∞, velocity U_∞ and yaw angle θ_∞ created between the fluid flow direction and x axis. The plate is considered to be composed of a homogeneous ceramic core and two non-symmetric FG face sheets which their properties vary from metal-rich layers to interior ceramic-rich ones according to two different power law functions. Thus,

volume fraction of the ceramic (V) can be considered as

$$\begin{cases} V^{(1)}(z)=\left(\dfrac{z-z_0}{z_1-z_0}\right)^p & for \quad z\in[z_0,z_1] \\ V^{(2)}(z)=1 & for \quad z\in[z_1,z_2] \\ V^{(3)}(z)=\left(\dfrac{z-z_3}{z_2-z_3}\right)^q & for \quad z\in[z_2,z_3] \end{cases} \tag{1}$$

where p and q are power law indices. A sample property of the plate (P) can be presented as

$$P(z)=P_m+(P_c-P_m)V(z) \tag{2}$$

in which subscripts "c" and "m" indicate corresponding properties in ceramic and metal, respectively. It should be noticed that usually in FG-structures Poisson's ratio (υ) is considered to be constant.

By introducing following dimensionless parameters

$$-1\le\xi=\frac{2z}{h}\le 1 \quad \xi_1=\frac{2z_1}{h} \quad \xi_2=\frac{2z_2}{h} \tag{3}$$

Eq. (1) can be written as

$$\begin{cases} V^{(1)}(\xi)=\left(\dfrac{\xi+1}{\xi_1+1}\right)^p & for \quad \xi\in[-1,\xi_1] \\ V^{(2)}(\xi)=1 & for \quad \xi\in[\xi_1,\xi_2] \\ V^{(3)}(\xi)=\left(\dfrac{\xi-1}{\xi_2-1}\right)^q & for \quad \xi\in[\xi_2,1] \end{cases} \tag{4}$$

and Eq. (2) can be written for elastic modulus (E) and density (ρ) as

$$\begin{aligned} E(\xi)&=E_m\left[1+(\mu_E-1)V(\xi)\right] \\ \rho(\xi)&=\rho_m\left[1+(\mu_\rho-1)V(\xi)\right] \end{aligned} \tag{5}$$

in which

$$\mu_E=\frac{E_c}{E_m} \quad \mu_\rho=\frac{\rho_c}{\rho_m} \tag{6}$$

The distance of the neutral axis from the mid-plane of the plate can be calculated as (Eltaher *et al*. 2013)

$$z_n=\frac{\int_{-\frac{h}{2}}^{\frac{h}{2}} zE(z)dz}{\int_{-\frac{h}{2}}^{\frac{h}{2}} E(z)dz} \tag{7}$$

which can be written in the following dimensionless form

$$\xi_n=\frac{2z_n}{h}=\frac{\int_{-1}^{1}\xi\left[1+(\mu_E-1)V(\xi)\right]d\xi}{\int_{-1}^{1}\left[1+(\mu_E-1)V(\xi)\right]d\xi} \tag{8}$$

According to the Reissner-Mindlin plate theory, the displacement field is considered as follows (Mindlin 1951)

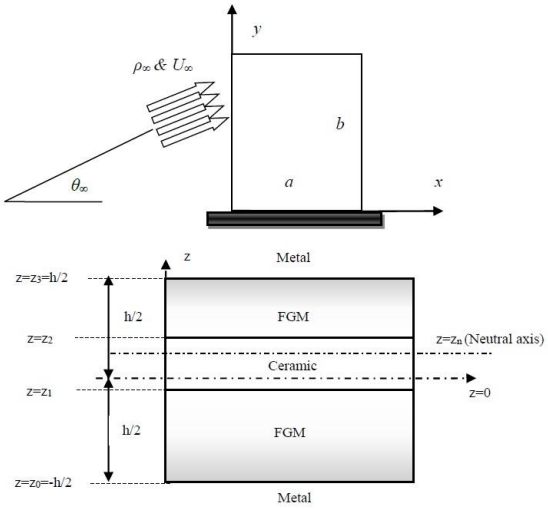

Fig. 1 Non-symmetric functionally graded sandwich plate in a compressible supersonic flow

$$\begin{aligned} u^z(x,y,z)&=u(x,y)+(z-z_n)\psi_x(x,y) \\ v^z(x,y,z)&=v(x,y)+(z-z_n)\psi_y(x,y) \\ w^z(x,y,z)&=w(x,y) \end{aligned} \tag{9}$$

where u^z, v^z and w^z show the components of displacement along x, y and z directions, respectively; u, v and w indicate corresponding components of displacement on the neutral axis ($z=z_n$) and ψ_x and ψ_y are rotations about y and x axes, respectively. Components of strain in plate can be stated as

$$\begin{aligned} \varepsilon_x&=\frac{\partial u}{\partial x}+(z-z_n)\frac{\partial\psi_x}{\partial x} \\ \varepsilon_y&=\frac{\partial v}{\partial y}+(z-z_n)\frac{\partial\psi_y}{\partial y} \\ \varepsilon_z&=0 \\ \gamma_{xy}&=\frac{\partial u}{\partial y}+\frac{\partial v}{\partial x}+(z-z_n)\left(\frac{\partial\psi_x}{\partial y}+\frac{\partial\psi_y}{\partial x}\right) \\ \gamma_{xz}&=\psi_x+\frac{\partial w}{\partial x} \\ \gamma_{yz}&=\psi_y+\frac{\partial w}{\partial y} \end{aligned} \tag{10}$$

Furthermore, by neglecting σ_z in comparison with σ_x and σ_y in Hook's laws, components of stress can be stated as

$$\begin{aligned} \sigma_x&=\frac{E}{1-\upsilon^2}\left[\frac{\partial u}{\partial x}+\upsilon\frac{\partial v}{\partial y}\right. \\ &\left.+(z-z_n)\left(\frac{\partial\psi_x}{\partial x}+\upsilon\frac{\partial\psi_y}{\partial y}\right)\right] \\ \sigma_y&=\frac{E}{1-\upsilon^2}\left[\frac{\partial v}{\partial y}+\upsilon\frac{\partial u}{\partial x}\right. \\ &\left.+(z-z_n)\left(\frac{\partial\psi_y}{\partial y}+\upsilon\frac{\partial\psi_x}{\partial x}\right)\right] \\ \sigma_z&=0 \\ \sigma_{xy}&=G\left[\frac{\partial u}{\partial y}+\frac{\partial v}{\partial x}+(z-z_n)\left(\frac{\partial\psi_x}{\partial y}+\frac{\partial\psi_y}{\partial x}\right)\right] \\ \sigma_{xz}&=kG\left(\psi_x+\frac{\partial w}{\partial x}\right) \\ \sigma_{yz}&=kG\left(\psi_y+\frac{\partial w}{\partial y}\right) \end{aligned} \tag{11}$$

in which k=(5+5υ)/(6+5υ) is shear correction factor (Kaneko 1975).

According to the Hamilton's principle, considering δ as variation operator, t as time and $[t_1,t_2]$ as a desired time interval, the set of governing equations and boundary conditions can be derived using following relation

$$\delta\int_{t_1}^{t_2}\left(T-U+W_{ext}\right)dt=0 \tag{12}$$

where T, U and W_{ext} are kinetic energy, strain energy and work done by external forces, respectively. These parameters are calculated as

$$\begin{aligned}
T&=\frac{1}{2}\iiint_V\rho\left[\left(\frac{\partial u^z}{\partial t}\right)^2+\left(\frac{\partial v^z}{\partial t}\right)^2+\left(\frac{\partial w^z}{\partial t}\right)^2\right]dV\\
U&=\frac{1}{2}\iiint_V\left(\sigma_x\varepsilon_x+\sigma_y\varepsilon_y+\sigma_z\varepsilon_z\right.\\
&\qquad\left.+\sigma_{xy}\gamma_{xy}+\sigma_{xz}\gamma_{xz}+\sigma_{yz}\gamma_{yz}\right)dV\\
W_{ext}&=\iint_S f\left(x,y,t\right)w\left(x,y,t\right)dS
\end{aligned} \tag{13}$$

in which V is volume of the plate, S is area of the plate at the middle surface and f is external force per unit area. By substituting Eqs. (9), (10) and (13) into Eq. (12), the set of governing equations can be derived as

$$\begin{aligned}
&\frac{\partial N_{xx}}{\partial x}+\frac{\partial N_{xy}}{\partial y}-I_0\frac{\partial^2 u}{\partial t^2}-I_1\frac{\partial^2\psi_x}{\partial t^2}=0\\
&\frac{\partial N_{yy}}{\partial y}+\frac{\partial N_{xy}}{\partial x}-I_0\frac{\partial^2 v}{\partial t^2}-I_1\frac{\partial^2\psi_y}{\partial t^2}=0\\
&\frac{\partial Q_{xz}}{\partial x}+\frac{\partial Q_{yz}}{\partial y}-I_0\frac{\partial^2 w}{\partial t^2}+f=0\\
&\frac{\partial M_{xx}}{\partial x}+\frac{\partial M_{xy}}{\partial y}-Q_{xz}-I_1\frac{\partial^2 u}{\partial t^2}-I_2\frac{\partial^2\psi_x}{\partial t^2}=0\\
&\frac{\partial M_{yy}}{\partial y}+\frac{\partial M_{xy}}{\partial x}-Q_{yz}-I_1\frac{\partial^2 v}{\partial t^2}-I_2\frac{\partial^2\psi_y}{\partial t^2}=0
\end{aligned} \tag{14}$$

and boundary conditions can be stated as follow

$$\begin{aligned}
x=0,a\qquad & y=0,b\\
N_{xx}\delta u=0\qquad & N_{xy}\delta u=0\\
N_{xy}\delta v=0\qquad & N_{yy}\delta v=0\\
Q_{xz}\delta w=0\qquad & Q_{yz}\delta w=0\\
M_{xx}\delta\psi_x=0\qquad & M_{xy}\delta\psi_x=0\\
M_{xy}\delta\psi_y=0\qquad & M_{yy}\delta\psi_y=0
\end{aligned} \tag{15}$$

where components of stress resultant and inertia are defined as

$$\begin{aligned}
\begin{Bmatrix}N_{xx}\\N_{yy}\\N_{xy}\end{Bmatrix}&=\int_{-\frac{h}{2}}^{\frac{h}{2}}\begin{Bmatrix}\sigma_x\\\sigma_y\\\sigma_{xy}\end{Bmatrix}dz\\
\begin{Bmatrix}M_{xx}\\M_{yy}\\M_{xy}\end{Bmatrix}&=\int_{-\frac{h}{2}}^{\frac{h}{2}}\begin{Bmatrix}\sigma_x\\\sigma_y\\\sigma_{xy}\end{Bmatrix}\left(z-z_n\right)dz\\
\begin{Bmatrix}Q_{xz}\\Q_{yz}\end{Bmatrix}&=\int_{-\frac{h}{2}}^{\frac{h}{2}}\begin{Bmatrix}\sigma_{xz}\\\sigma_{yz}\end{Bmatrix}dz
\end{aligned} \tag{16}$$

$$\begin{Bmatrix}I_0\\I_1\\I_2\end{Bmatrix}=\int_{-\frac{h}{2}}^{\frac{h}{2}}\begin{Bmatrix}1\\z-z_n\\\left(z-z_n\right)^2\end{Bmatrix}\rho dz$$

Using Eqs. (11) and (16) one can write

$$\begin{aligned}
N_{xx}&=A\left(\frac{\partial u}{\partial x}+\upsilon\frac{\partial v}{\partial y}\right)+B\left(\frac{\partial\psi_x}{\partial x}+\upsilon\frac{\partial\psi_y}{\partial y}\right)\\
N_{yy}&=A\left(\frac{\partial v}{\partial y}+\upsilon\frac{\partial u}{\partial x}\right)+B\left(\frac{\partial\psi_y}{\partial y}+\upsilon\frac{\partial\psi_x}{\partial x}\right)\\
N_{xy}&=\upsilon_1\left[A\left(\frac{\partial u}{\partial y}+\frac{\partial v}{\partial x}\right)+B\left(\frac{\partial\psi_x}{\partial y}+\frac{\partial\psi_y}{\partial x}\right)\right]\\
M_{xx}&=B\left(\frac{\partial u}{\partial x}+\upsilon\frac{\partial v}{\partial y}\right)+D\left(\frac{\partial\psi_x}{\partial x}+\upsilon\frac{\partial\psi_y}{\partial y}\right)\\
M_{yy}&=B\left(\frac{\partial v}{\partial y}+\upsilon\frac{\partial u}{\partial x}\right)+D\left(\frac{\partial\psi_y}{\partial y}+\upsilon\frac{\partial\psi_x}{\partial x}\right)\\
M_{xy}&=\upsilon_1\left[B\left(\frac{\partial u}{\partial y}+\frac{\partial v}{\partial x}\right)+D\left(\frac{\partial\psi_x}{\partial y}+\frac{\partial\psi_y}{\partial x}\right)\right]\\
Q_{xz}&=k\upsilon_1 A\left(\psi_x+\frac{\partial w}{\partial x}\right)\\
Q_{yz}&=k\upsilon_1 A\left(\psi_y+\frac{\partial w}{\partial y}\right)
\end{aligned} \tag{17}$$

in which

$$\begin{Bmatrix}A\\B\\D\end{Bmatrix}=\int_{-\frac{h}{2}}^{\frac{h}{2}}\frac{E\left(z\right)}{1-\upsilon^2}\begin{Bmatrix}1\\z-z_n\\\left(z-z_n\right)^2\end{Bmatrix}dz\quad \upsilon_1=\frac{1-\upsilon}{2} \tag{18}$$

For flutter analysis, the external force per unit area is created by the aerodynamic load. For the Mach numbers in the range of M_∞>1.7, this load is approximately evaluated by the supersonic piston theory (Grover *et al.* 2016)

$$f=-\xi_\infty\left(\frac{\partial w}{\partial x}\cos\theta_\infty+\frac{\partial w}{\partial y}\sin\theta_\infty\right)-\mu_\infty\frac{\partial w}{\partial t} \tag{19}$$

in which ξ_∞ and μ_∞ are the aerodynamic pressure and damping parameters, respectively; these parameters are presented as

$$\xi_\infty=\frac{\rho_\infty U_\infty^2}{\sqrt{M_\infty^2-1}}\quad \mu_\infty=\frac{\rho_\infty U_\infty\left(M_\infty^2-2\right)}{\sqrt{\left(M_\infty^2-1\right)^3}} \tag{20}$$

As the aerodynamic damping term in Eq. (19) always stabilizes the flutter boundaries (Shin et al. 2006), to study the aeroelastic characteristics of supersonic plate, the aerodynamic load without the aerodynamic damping is used to derive the flutter equation of the supersonic plate (Shin *et al.* 2006). Thus, substituting Eqs. (17) and (19) into the Eq. (14) and neglecting aerodynamic damping, the set of governing equations can be stated as

$$
\begin{aligned}
&A\frac{\partial^2 u}{\partial x^2}+\upsilon_1 A\frac{\partial^2 u}{\partial y^2}+\upsilon_2 A\frac{\partial^2 v}{\partial x\partial y}+B\frac{\partial^2 \psi_x}{\partial x^2}\\
&+\upsilon_1 B\frac{\partial^2 \psi_x}{\partial y^2}+\upsilon_2 B\frac{\partial^2 \psi_y}{\partial x\partial y}=I_0\frac{\partial^2 u}{\partial t^2}+I_1\frac{\partial^2 \psi_x}{\partial t^2}\\
&\upsilon_2 A\frac{\partial^2 u}{\partial x\partial y}+\upsilon_1 A\frac{\partial^2 v}{\partial x^2}+A\frac{\partial^2 v}{\partial y^2}+\upsilon_2 B\frac{\partial^2 \psi_x}{\partial x\partial y}\\
&+\upsilon_1 B\frac{\partial^2 \psi_y}{\partial x^2}+B\frac{\partial^2 \psi_y}{\partial y^2}=I_0\frac{\partial^2 v}{\partial t^2}+I_1\frac{\partial^2 \psi_y}{\partial t^2}\\
&k\upsilon_1 A\left(\frac{\partial^2 w}{\partial x^2}+\frac{\partial^2 w}{\partial y^2}+\frac{\partial \psi_x}{\partial x}+\frac{\partial \psi_y}{\partial y}\right)\\
&-\xi_\infty\left(\frac{\partial w}{\partial x}\cos\theta_\infty+\frac{\partial w}{\partial y}\sin\theta_\infty\right)=I_0\frac{\partial^2 w}{\partial t^2}\\
&B\frac{\partial^2 u}{\partial x^2}+\upsilon_1 B\frac{\partial^2 u}{\partial y^2}+\upsilon_2 B\frac{\partial^2 v}{\partial x\partial y}-k\upsilon_1 A\frac{\partial w}{\partial x}\\
&+D\frac{\partial^2 \psi_x}{\partial x^2}+\upsilon_1 D\frac{\partial^2 \psi_x}{\partial y^2}-k\upsilon_1 A\psi_x\\
&+\upsilon_2 D\frac{\partial^2 \psi_y}{\partial x\partial y}=I_1\frac{\partial^2 u}{\partial t^2}+I_2\frac{\partial^2 \psi_x}{\partial t^2}\\
&\upsilon_2 B\frac{\partial^2 u}{\partial x\partial y}+\upsilon_1 B\frac{\partial^2 v}{\partial x^2}+B\frac{\partial^2 v}{\partial y^2}-k\upsilon_1 A\frac{\partial w}{\partial y}\\
&+\upsilon_2 D\frac{\partial^2 \psi_x}{\partial x\partial y}+\upsilon_1 D\frac{\partial^2 \psi_y}{\partial x^2}+D\frac{\partial^2 \psi_y}{\partial y^2}\\
&-k\upsilon_1 A\psi_y=I_1\frac{\partial^2 v}{\partial t^2}+I_2\frac{\partial^2 \psi_y}{\partial t^2}
\end{aligned}
\tag{21}
$$

in which $\upsilon_2=(1+\upsilon)/2$. For the cantilever plate depicted in Fig. 1, boundary conditions can be considered as

$$
\begin{array}{lll}
y=0: & y=b: & x=0,a:\\
u=0 & N_{xy}=0 & N_{xx}=0\\
v=0 & N_{yy}=0 & N_{xy}=0\\
w=0 & Q_{yz}=0 & Q_{xz}=0\\
\psi_x=0 & M_{xy}=0 & M_{xx}=0\\
\psi_y=0 & M_{yy}=0 & M_{xy}=0
\end{array}
\tag{22}
$$

and using Eqs. (17) and (22) boundary conditions at free edges can be written as

$$
\begin{aligned}
&y=b:\\
&A\left(\frac{\partial u}{\partial y}+\frac{\partial v}{\partial x}\right)+B\left(\frac{\partial \psi_x}{\partial y}+\frac{\partial \psi_y}{\partial x}\right)=0\\
&A\left(\frac{\partial v}{\partial y}+\upsilon\frac{\partial u}{\partial x}\right)+B\left(\frac{\partial \psi_y}{\partial y}+\upsilon\frac{\partial \psi_x}{\partial x}\right)=0\\
&\psi_y+\frac{\partial w}{\partial y}=0\\
&B\left(\frac{\partial u}{\partial y}+\frac{\partial v}{\partial x}\right)+D\left(\frac{\partial \psi_x}{\partial y}+\frac{\partial \psi_y}{\partial x}\right)=0\\
&B\left(\frac{\partial v}{\partial y}+\upsilon\frac{\partial u}{\partial x}\right)+D\left(\frac{\partial \psi_y}{\partial y}+\upsilon\frac{\partial \psi_x}{\partial x}\right)=0
\end{aligned}
\tag{23}
$$

$$
\begin{aligned}
&x=0,a:\\
&A\left(\frac{\partial u}{\partial x}+\upsilon\frac{\partial v}{\partial y}\right)+B\left(\frac{\partial \psi_x}{\partial x}+\upsilon\frac{\partial \psi_y}{\partial y}\right)=0\\
&A\left(\frac{\partial u}{\partial y}+\frac{\partial v}{\partial x}\right)+B\left(\frac{\partial \psi_x}{\partial y}+\frac{\partial \psi_y}{\partial x}\right)=0\\
&\psi_x+\frac{\partial w}{\partial x}=0\\
&B\left(\frac{\partial u}{\partial x}+\upsilon\frac{\partial v}{\partial y}\right)+D\left(\frac{\partial \psi_x}{\partial x}+\upsilon\frac{\partial \psi_y}{\partial y}\right)=0\\
&B\left(\frac{\partial u}{\partial y}+\frac{\partial v}{\partial x}\right)+D\left(\frac{\partial \psi_x}{\partial y}+\frac{\partial \psi_y}{\partial x}\right)=0
\end{aligned}
$$

which can be simplified to

$$
\begin{array}{ll}
y=b: & x=0,a:\\
\dfrac{\partial u}{\partial y}+\dfrac{\partial v}{\partial x}=0 & \dfrac{\partial u}{\partial x}+\upsilon\dfrac{\partial v}{\partial y}=0\\
\dfrac{\partial v}{\partial y}+\upsilon\dfrac{\partial u}{\partial x}=0 & \dfrac{\partial u}{\partial y}+\dfrac{\partial v}{\partial x}=0\\
\psi_y+\dfrac{\partial w}{\partial y}=0 & \psi_x+\dfrac{\partial w}{\partial x}=0\\
\dfrac{\partial \psi_x}{\partial y}+\dfrac{\partial \psi_y}{\partial x}=0 & \dfrac{\partial \psi_x}{\partial x}+\upsilon\dfrac{\partial \psi_y}{\partial y}=0\\
\dfrac{\partial \psi_y}{\partial y}+\upsilon\dfrac{\partial \psi_x}{\partial x}=0 & \dfrac{\partial \psi_x}{\partial y}+\dfrac{\partial \psi_y}{\partial x}=0
\end{array}
\tag{24}
$$

Using Eqs. (3), (5), (16) and (18), following relations can be presented

$$
\begin{array}{lll}
A=A_m f_0 & B=B_m f_1 & D=D_m f_2\\
I_0=I_{0m}g_0 & I_1=I_{1m}g_1 & I_2=I_{2m}g_2
\end{array}
\tag{25}
$$

where equivalent forms of rigidity and inertia of a pure metallic plate are defined as

$$
\begin{array}{ll}
A_m=\dfrac{E_m h}{1-\upsilon^2} & I_{0m}=\rho_m h\\
B_m=\dfrac{E_m h^2}{4\left(1-\upsilon^2\right)} & I_{1m}=\dfrac{\rho_m h^2}{4}\\
D_m=\dfrac{E_m h^3}{12\left(1-\upsilon^2\right)} & I_{2m}=\dfrac{\rho_m h^3}{12}
\end{array}
\tag{26}
$$

and f_0-g_2 are coefficients defined as

$$
f_0=\frac{1}{2}\int_{-1}^{1}\left[1+\left(\mu_E-1\right)V\left(\xi\right)\right]d\xi
\tag{27}
$$

$$f_1=\int_{-1}^{1}\left[1+(\mu_E-1)V(\xi)\right](\xi-\xi_0)d\xi$$
$$f_2=\frac{3}{2}\int_{-1}^{1}\left[1+(\mu_E-1)V(\xi)\right](\xi-\xi_0)^2 d\xi$$
$$g_0=\frac{1}{2}\int_{-1}^{1}\left[1+(\mu_\rho-1)V(\xi)\right]d\xi$$
$$g_1=\int_{-1}^{1}\left[1+(\mu_\rho-1)V(\xi)\right](\xi-\xi_0)d\xi$$
$$g_2=\frac{3}{2}\int_{-1}^{1}\left[1+(\mu_\rho-1)V(\xi)\right](\xi-\xi_0)^2 d\xi$$

Using dimensionless variables ζ=x/a and η=y/b and using the method of separation of variables as

$$\begin{Bmatrix} u(\zeta,\eta,t)\\ v(\zeta,\eta,t)\\ w(\zeta,\eta,t)\\ \psi_x(\zeta,\eta,t)\\ \psi_y(\zeta,\eta,t)\end{Bmatrix}=\begin{Bmatrix} bU(\zeta,\eta)\\ bV(\zeta,\eta)\\ bW(\zeta,\eta)\\ X(\zeta,\eta)\\ Y(\zeta,\eta)\end{Bmatrix}e^{\omega t} \tag{28}$$

where ω is an eigen value, the set of governing Eq. (21) can be rewritten as

$$\begin{aligned}
&\frac{12f_0}{\gamma}U_{,\zeta\zeta}+\frac{12\upsilon_1\phi^2 f_0}{\gamma}U_{,\eta\eta}+\frac{12\upsilon_2\phi f_0}{\gamma}V_{,\zeta\eta}\\
&+3f_1X_{,\zeta\zeta}+3\upsilon_1\phi^2 f_1X_{,\eta\eta}+3\upsilon_2\phi f_1Y_{,\zeta\eta}\\
&=\lambda^2\gamma\phi^2\left(g_0U+\frac{\gamma g_1}{4}X\right)\\
&\frac{12\upsilon_2\phi f_0}{\gamma}U_{,\zeta\eta}+\frac{12\upsilon_1 f_0}{\gamma}V_{,\zeta\zeta}+\frac{12\phi^2 f_0}{\gamma}V_{,\eta\eta}\\
&+3\upsilon_2\phi f_1X_{,\zeta\eta}+3\upsilon_1 f_1Y_{,\zeta\zeta}+3\phi^2 f_1Y_{,\eta\eta}\\
&=\lambda^2\gamma\phi^2\left(g_0V+\frac{\gamma g_1}{4}Y\right)\\
&-\frac{12k\upsilon_1 f_0}{\gamma}\left(W_{,\zeta\zeta}+\phi^2W_{,\eta\eta}+\phi X_{,\zeta}+\phi^2Y_{,\eta}\right)\\
&+\frac{\xi_\infty^* m_\infty}{\gamma^2}\left(\phi W_{,\zeta}\cos\theta_\infty+\phi^2W_{,\eta}\sin\theta_\infty\right)\\
&=-\lambda^2\gamma\phi^2g_0W\\
&3f_1U_{,\zeta\zeta}+3\upsilon_1\phi^2 f_1U_{,\eta\eta}+3\upsilon_2\phi f_1V_{,\zeta\eta}\\
&-\frac{12k\upsilon_1\phi f_0}{\gamma}W_{,\zeta}+\gamma f_2X_{,\zeta\zeta}+\upsilon_1\gamma\phi^2 f_2X_{,\eta\eta}\\
&-\frac{12k\upsilon_1\phi^2 f_0}{\gamma}X+\upsilon_2\gamma\phi f_2Y_{,\zeta\eta}\\
&=\frac{\lambda^2\gamma^2\phi^2}{4}\left(g_1U+\frac{\gamma g_2}{3}X\right)\\
&3\upsilon_2\phi f_1U_{,\zeta\eta}+3\upsilon_1 f_1V_{,\zeta\zeta}+3\phi^2 f_1V_{,\eta\eta}\\
&-\frac{12k\upsilon_1\phi^2 f_0}{\gamma}W_{,\eta}+\upsilon_2\gamma\phi f_2X_{,\zeta\eta}+\upsilon_1\gamma f_2Y_{,\zeta\zeta}\\
&+\gamma\phi^2 f_2Y_{,\eta\eta}-\frac{12k\upsilon_1\phi^2 f_0}{\gamma}Y\\
&=\frac{\lambda^2\gamma^2\phi^2}{4}\left(g_1V+\frac{\gamma g_2}{3}Y\right)
\end{aligned} \tag{29}$$

where following dimensionless parameters are defined

$$\phi=\frac{a}{b}\quad\gamma=\frac{h}{b}$$
$$\xi_\infty^*=12\left(1-\upsilon^2\right)\frac{\rho_\infty U_s^2}{E_m}\quad m_\infty=\frac{M_\infty^2}{\sqrt{M_\infty^2-1}} \tag{30}$$
$$\lambda^2=\frac{\rho_m hb^4\omega^2}{D_m}$$

in which U_s is the velocity of sound. Also dimensionless form of boundary conditions can be stated as

$$\begin{array}{lll}
\eta=0: & \eta=1: & \zeta=0,1:\\
U=0 & \phi U_{,\eta}+V_{,\zeta}=0 & U_{,\zeta}+\phi\upsilon V_{,\eta}=0\\
V=0 & \upsilon U_{,\zeta}+\phi V_{,\eta}=0 & \phi U_{,\eta}+V_{,\zeta}=0\\
W=0 & W_{,\eta}+Y=0 & W_{,\zeta}+\phi X=0\\
X=0 & \phi X_{,\eta}+Y_{,\zeta}=0 & X_{,\zeta}+\upsilon\phi Y_{,\eta}=0\\
Y=0 & \upsilon X_{,\zeta}+\phi Y_{,\eta}=0 & \phi X_{,\eta}+Y_{,\zeta}=0
\end{array} \tag{31}$$

3. Differential quadrature method

Values of function F(ζ,η) at N×M pre-selected grid of points can be considered as

$$\begin{aligned}
&F_{ij}=F\left(\zeta_i,\eta_j\right)\\
&i=1,2,...,N\quad j=1,2,...,M
\end{aligned} \tag{32}$$

According to the differential quadrature rules, all derivatives of the function can be approximated by means of weighted linear sum of the function values at the pre-selected grid of points as

$$\begin{aligned}
\left.\frac{\partial F}{\partial\zeta}\right|_{(\zeta,\eta)=(\zeta_i,\eta_j)}&=\sum_{n=1}^{N}A_{in}^{(\zeta)}F_{nj}\\
\left.\frac{\partial^2 F}{\partial\zeta^2}\right|_{(\zeta,\eta)=(\zeta_i,\eta_j)}&=\sum_{n=1}^{N}B_{in}^{(\zeta)}F_{nj}\\
\left.\frac{\partial F}{\partial\eta}\right|_{(\zeta,\eta)=(\zeta_i,\eta_j)}&=\sum_{m=1}^{M}A_{jm}^{(\eta)}F_{im}\\
\left.\frac{\partial^2 F}{\partial\eta^2}\right|_{(\zeta,\eta)=(\zeta_i,\eta_j)}&=\sum_{m=1}^{M}B_{jm}^{(\eta)}F_{im}
\end{aligned} \tag{33}$$

$$\left.\frac{\partial^2 F}{\partial\zeta\partial\eta}\right|_{(\zeta,\Theta)=(\zeta_i,\eta_j)}=\sum_{n=1}^{N}A_{in}^{(\zeta)}\sum_{m=1}^{M}A_{jm}^{(\eta)}F_{nm}$$

where $A^{(\zeta)}$, $B^{(\zeta)}$, $A^{(\eta)}$ and $B^{(\eta)}$ are the weighting coefficients associated with the first and second order derivatives in ζ and η directions, respectively. These matrices for the first-order derivatives are given as (Bert and Malik 1996)

$$A_{in}^{(\zeta)}=\begin{cases}\dfrac{\prod_{\substack{k=1\\k\neq i,n}}^{N}(\zeta_i-\zeta_k)}{\prod_{\substack{k=1\\k\neq n}}^{N}(\zeta_n-\zeta_k)}, & (i,n=1,2,3,...,N;i\neq n)\\ \sum_{\substack{k=1\\k\neq i}}^{N}\dfrac{1}{(\zeta_i-\zeta_k)}, & (i=n=1,2,3,...,N)\end{cases}$$

$$A_{jm}^{(\eta)}=\begin{cases}\dfrac{\prod_{\substack{k=1\\k\neq j,m}}^{M}(\eta_j-\eta_k)}{\prod_{\substack{k=1\\k\neq m}}^{M}(\eta_m-\eta_k)}, & (j,m=1,2,3,...,M;j\neq m)\\ \sum_{\substack{k=1\\k\neq j}}^{M}\dfrac{1}{(\eta_j-\eta_k)}, & (j=m=1,2,3,...,M)\end{cases} \tag{34}$$

and of second-order derivatives are extracted from the following relations

$$B^{(\zeta)}=A^{(\zeta)}A^{(\zeta)}\quad B^{(\eta)}=A^{(\eta)}A^{(\eta)} \tag{35}$$

Eq. (37) can be written in the following matrix form

$$\begin{aligned}&\left[F_{,\zeta}\right]=\left[A^{(\zeta)}\right][F]\quad \left[F_{,\zeta\zeta}\right]=\left[B^{(\zeta)}\right][F]\\ &\left[F_{,\eta}\right]=[F]\left[A^{(\eta)}\right]^T\quad \left[F_{,\eta\eta}\right]=[F]\left[B^{(\eta)}\right]^T\\ &\left[F_{,\zeta\eta}\right]=\left[A^{(\zeta)}\right][F]\left[B^{(\eta)}\right]^T\end{aligned} \tag{36}$$

in which superscript T indicates transpose operator.

For a matrix $[F]_{N\times M}$, an equivalent column vector $\{\bar{F}\}_{NM\times 1}$ can be defined as (Torabi and Afshari 2017a)

$$\bar{F}_v=F_{ij}\quad v=(j-1)N+i \tag{37}$$

Using this technique, multiple of three matrices as $[a][F][b]$ can be replaced by $\left([b]^T\otimes[a]\right)\{\bar{F}\}$; in which $\otimes$ indicates the Kronecker product (Torabi and Afshari 2017a). Therefore, Eq. (40) can be written as

$$\begin{aligned}&\left\{\bar{F}_{,\zeta}\right\}=\left(I^{(\eta)}\otimes\left[A^{(\zeta)}\right]\right)\{\bar{F}\}\\ &\left\{\bar{F}_{,\zeta\zeta}\right\}=\left(I^{(\eta)}\otimes\left[B^{(\zeta)}\right]\right)\{\bar{F}\}\\ &\left\{\bar{F}_{,\eta}\right\}=\left(\left[A^{(\eta)}\right]\otimes I^{(\zeta)}\right)\{\bar{F}\}\\ &\left\{\bar{F}_{,\eta\eta}\right\}=\left(\left[B^{(\eta)}\right]\otimes I^{(\zeta)}\right)\{\bar{F}\}\\ &\left\{\bar{F}_{,\zeta\eta}\right\}=\left(\left[A^{(\eta)}\right]\otimes\left[A^{(\zeta)}\right]\right)\{\bar{F}\}\end{aligned} \tag{38}$$

where $I^{(\zeta)}$ and $I^{(\eta)}$ indicate the identity matrices of order N and M, respectively.

In addition to number of grid points, distribution of them affects convergence of solution. A well-accepted set of the grid points is the Gauss–Lobatto–Chebyshev points given for interval [0,1] as (Bert and Malik 1996)

$$\begin{aligned}&\zeta_i=\frac{1}{2}\left\{1-\cos\left[\frac{(i-1)\pi}{(N-1)}\right]\right\}\quad i=1,2,...,N\\ &\eta_j=\frac{1}{2}\left\{1-\cos\left[\frac{(j-1)\pi}{M-1}\right]\right\}\quad j=1,2,...,M\end{aligned} \tag{39}$$

4. DQ analogue

Using DQ rules, the set of governing differential Eq. (29) is transformed to the following form

$$[K]\{s\}=\lambda^2[M]\{s\} \tag{40}$$

where [K] and [M] are stiffness and mass matrices which are presented in details in Appendix A. Also in a similar manner boundary conditions (31) can be written using DQ rules as

$$[T]\{u\}=\{0\} \tag{41}$$

in which matrix [T] is presented in details in Appendix B.

The grid points can be separated into two sets: boundary points which are located at the four edges of the plate and domain ones which are other internal points. By neglecting satisfying the Eq. (40) at the boundary points, this equation can be written as (Du *et al.* 1994)

$$\left[\bar{K}\right]\{s\}=\lambda^2\left[\bar{M}\right]\{s\} \tag{42}$$

where bar sign implies the corresponding non-square matrix. Eqs. (41) and (42) may be rearranged and partitioned in order to separate the boundary (b) and domain (d) points as follows

$$\begin{aligned}&\left[\bar{K}\right]_d\{s\}_d+\left[\bar{K}\right]_b\{s\}_b\\ &=\lambda^2\left(\left[\bar{M}\right]_d\{s\}_d+\left[\bar{M}\right]_b\{s\}_b\right)\end{aligned} \tag{43a}$$

$$[T]_d\{s\}_d+[T]_b\{s\}_b=\{0\} \tag{43b}$$

Substituting Eq. (43(b)) into Eq. (43(a)) leads to the following eigen value equation

$$[K_t]\{s\}_d=\lambda^2[M_t]\{s\}_d \tag{44}$$

in which

Table 1 Mechanical properties of the materials used in the FG sandwich plate (Hosseini-Hashemi *et al*. 2011)

Material		Properties		
		E (GPa)	ρ (kg/m^3)	υ
Aluminum (Al)	Metal	70	2702	0.3
Alumina (Al_2O_3)	Ceramic	380	3800	0.3

Table 2 Convergence of the presented solution

N=M	5	7	9	11	13	15	17	19	21
Ω_1	7.774074	6.125260	6.223997	6.257455	6.273370	6.281024	6.284421	6.285821	6.286373
Ω_2	29.80827	11.96498	10.46085	9.932952	9.693708	9.566213	9.494072	9.451423	9.425048
Ω_3	113.5690	11.96498	19.05531	18.48284	18.10157	17.88133	17.75882	17.69121	17.65318
Ω_4	207.4183	18.65217	32.37174	33.52119	33.54693	33.31259	33.15478	33.05720	32.99643

Table 3 Non-dimensional critical aerodynamic pressure and non-dimensional flutter frequencies for a homogeneous square plate

χ_{cr}			Ω_{cr}		
Present	FEM (Chowdary et al. 1996)	FEM (Singha and Ganapathi 2005)	Present	FEM (Chowdary et al. 1996)	FEM (Singha and Ganapathi 2005)
61.75	59.51	57.89	6.7	6.48	-

$$[K_t]=[\bar{K}]_d-[\bar{K}]_b[T]_b^{-1}[T]_d$$
$$[M_t]=[\bar{M}]_d-[\bar{M}]_b[T]_b^{-1}[T]_d \quad (45)$$

It should be noted that the eigen values achieved using Eq. (44) are complex numbers. Non-dimensional frequencies (Ω) are defined as imaginary part of eigen values $\Omega=\mathrm{Im}(\lambda)$ and the real part of eigen values specify stability or instability of oscillation.

5. Numerical results

A numerical investigation was presented in previous sections for supersonic flutter analysis of non-symmetric FG sandwich plates. In this section, numerical examples are presented for the presented solution. Unless mentioned otherwise, numerical results are reported for a functionally graded sandwich plate composed of aluminum as metal and alumina as ceramic which their mechanical properties are presented in Table 1.

At first, convergence and accuracy of the presented numerical solution should be tested. For this purpose, consider a sandwich plate of $\varphi=2$, $\gamma=0.02$, $\xi_1=-0.6$, $\xi_2=0.8$, $p=0.5$ and $q=1.5$ exposed to a supersonic flow of $\xi^*_\infty=2\times10^{-5}$, $M_\infty=3$, and $\theta_\infty=15°$. Effect of the number of grid points (N=M) on the values of the first four dimensionless frequencies of the plate is presented in Table 2. This table confirms convergence of the proposed numerical solution and N=M=15 is considered in all of the following numerical examples.

In order to validate the proposed numerical solution consider a homogeneous plate of $\varphi=1$ and $\gamma=0.01$. Variation of first two dimensionless frequencies and corresponding real parts versus variation of non-dimensional aerodynamic pressure ($\chi=\rho_\infty U_s^2 a^3 M_\infty^2 \Big/ D_c\sqrt{M_\infty^2-1}$) are depicted Figs. 3(a) and 3(b). As shown in these figures, increase in aerodynamic pressure leads to increase in first frequency and decrease in second one. At $\chi=61.75$ these two

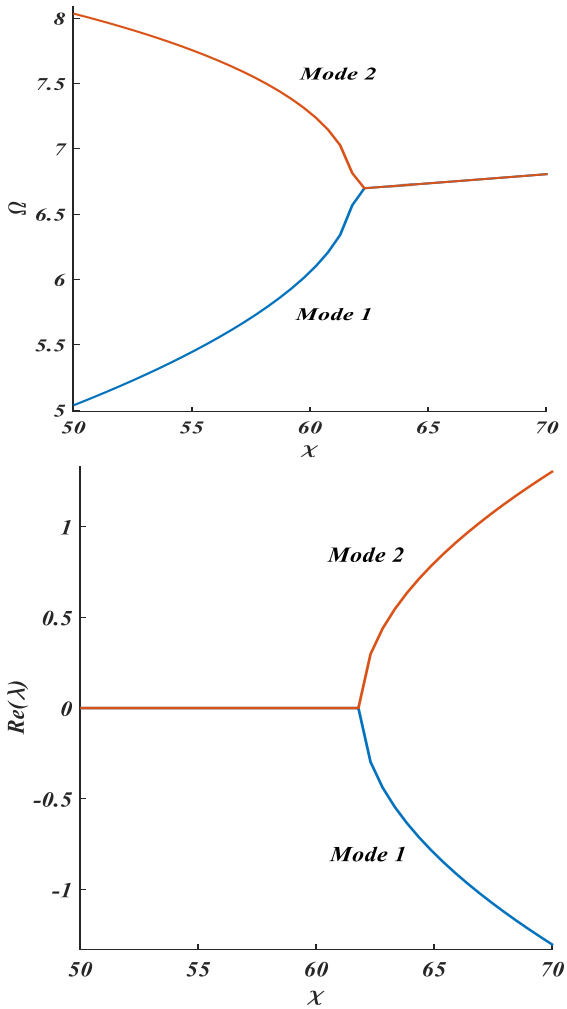

Fig. 2 Effect of aerodynamic pressure on values of the first two frequencies and corresponding real parts of a homogeneous square plate

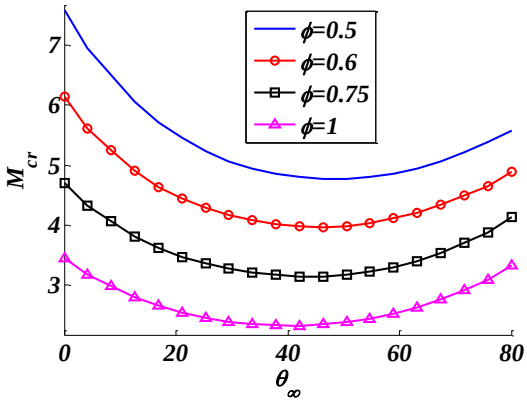

Fig. 3 Effect of aspect ratio on critical Mach number

frequencies become equal to Ω=6.7 and corresponding value of real part of the second mode becomes a positive value. In fact, at this point, the aeroelastic self-excited oscillation of the plate occurs which is known as the flutter. Value of the aerodynamic pressure at this point is called critical aerodynamic pressure and the corresponding frequency is called the flutter frequency.

At Table 3, values of the non-dimensional critical aerodynamic pressure and non-dimensional flutter frequencies are listed and compared with those presented by other authors based on FEM. This comparison confirms the high accuracy of the presented solution.

Convergence and accuracy of the presented numerical solution were confirmed by Tables 2 and 3. In what follows a parametric study is presented for study the effect of different parameters on flutter boundaries of the sandwich plates. For all of the following example the plates is considered to be exposed to a supersonic flow of $\xi^*_\infty=5\times10^{-5}$.

In order to investigate effect of aspect ratio on flutter boundaries, consider a sandwich plate of γ=0.01, ξ_1=-0.7, ξ_2=0.3, p=1 and q=2. Fig. 3 shows variation of critical velocity versus variation of yaw angle for various values of aspect ratio. This figure shows that for all values of the yaw angle, increase in value of aspect ratio decreases value of the critical speed and plates with lower aspect ratio are more stable for all values of yaw angle. In other words, for all values of the yaw angle, wings and tail fins with longer length and shorter width are more stable against supersonic flows.

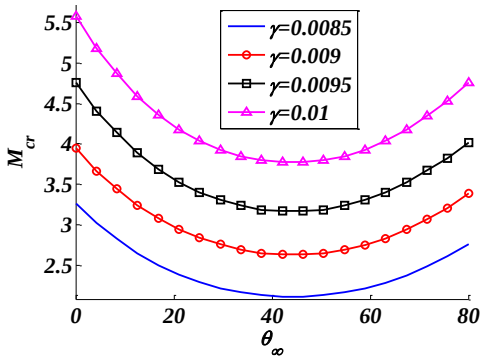

Fig. 4 Effect of total thickness of the plate on critical Mach number

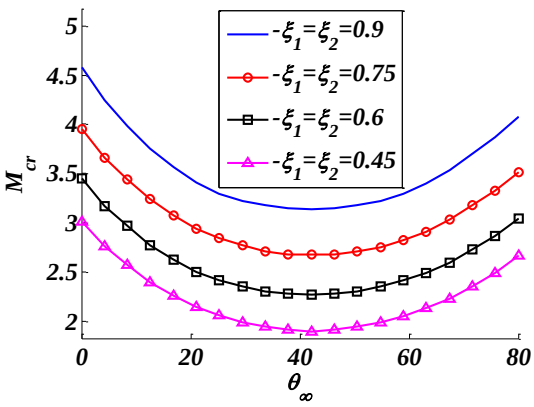

Fig. 5 Effect of relative thickness of core and FG face sheets on critical Mach number

Thickness of the plate has a significant effect on aeroelastic behavior of the plate. For investigate this aspect, a sandwich plate of φ=0.8, ξ_1=-0.3, ξ_2=0.5, p=0.75 and q=1 is considered. For different values of dimensionless thickness of the plate, variation of critical speed versus variation of yaw angle is depicted in Fig. 4. As shown in this figure, for all values of the yaw angle a small grow in thickness of the plate can lead to a considerable rise in value of the critical speed. Although it can be concluded that thicker plates are more stable against supersonic flows, but it should be noted that increase in thickness of the plate makes it heavier which is not a suitable item for aircrafts.

Flutter boundaries of the sandwich plate can be affected by change in thickness of the homogeneous ceramic core and FG face sheets. Consider a geometrically symmetric sandwich plate (ξ_2=-ξ_1) of φ=0.7, γ=0.008, p=1.5 and q=0.25. In Fig. 5 variation of critical speed versus variation of yaw angle is depicted for different values of thickness of FG face sheets. This figure reveals that in order to increase value of critical speed and expand flutter boundaries for any values of the yaw angle, it is better to increase thickness of the ceramic core and decrease thickness of FG face sheets. In other words increase in volume fraction of ceramic makes the plate more stable. But Table 1 shows that this attempt increases total weight of the plate.

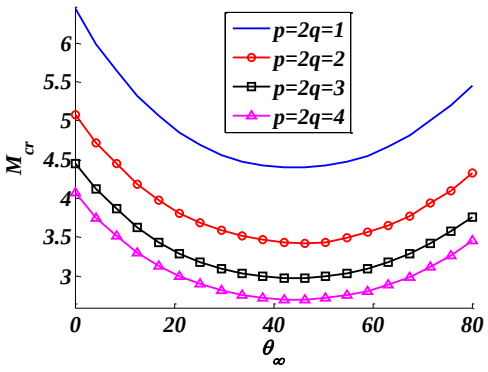

Fig. 6 Effect of power law indices on critical Mach number

In order to study the effect of power law indices on the aeroelastic characteristics of FG sandwich plates, a sandwich plate of φ=0.8, γ=0.01, ξ_1=-0.5 and ξ_2=0.5 is considered. For various values of p and q, variation of critical speed versus variation of follow angle is depicted in Fig. 6. This figure reveals that for all values of the yaw angle increase in value of p and q leads to decrease in value of critical speed of the plate. According to Eq. (1) it can be claimed that decrease in values of volume fraction of ceramic in FG face sheets decreases the aeroelastic stability of the plate which is in agreement with those was concluded using Fig. 5.

Figs. 3-6 shows that as yaw angle increases, value of the critical speed decreases at first and then increases. Thus there is a critical value for yaw angle which minimize value of critical speed. Figs. 3-6 reveal that increase in value of the aspect ratio (decrease in length and increase in width of the plate) decreases value of the critical yaw angle and other parameters such as total thickness of the plate, relative thickness of core and face sheets and also power law indices have no remarkable effect on value of critical yaw angle.

6. Conclusions

Using GDQM a numerical solution was presented for aeroelastic stability analysis of cantilever sandwich plates with homogenous core and non-symmetric FG face sheets. The plate was modeled based on the FSDT and aerodynamic load was calculated using the linear piston theory. Numerical results were presented for sandwich plates made of Al-Al_2O_3, and effects of yaw angle, aspect ratio, thickness of the plate, thickness of the cramic core and FG face sheets and also power law indices on the flutter boundaries were investigated. Numerical results revealed that in order to expand flutter boundaries of cantilever plates, it is better to use ones with larger length and shorter width, as much as possible. It was shown that increase in volume fraction of ceramic (Al_2O_3) makes the plate more stable; but increases the total mass of the plate, as well. It was concluded that value of the critical yaw angle depends only on value of the aspect ratio and other parameters have no remarkable effect on it.

References

Afshari, H. and Torabi, K. (2017), "A parametric study on flutter analysis of cantilevered trapezoidal FG sandwich plates", *Amirkabir J. Sci. Res. Mech. Eng.*, **1**(2), 191-210.

Bert, C.W. and Malik, M. (1996), "Differential quadrature method in computational mechanics: a review", *Appl. Mech. Review.*, **49**(1), 1-28. https://doi.org/10.1115/1.3101882.

Chowdary, T., Sinha, P. and Parthan, S. (1996), "Finite element flutter analysis of composite skew panels", *Comput. Struct.*, **58**(3), 613-620. https://doi.org/10.1016/0045-7949(95)00153-8.

Cunha-Filho, A., De Lima, A., Donadon, M. and Leão, L. (2016), "Flutter suppression of plates using passive constrained viscoelastic layers", *Mech. Syst. Signal Pr.*, **79**, 99-111. https://doi.org/10.1016/j.ymssp.2016.02.025.

Du, H., Lim, M. and Lin, R. (1994), "Application of generalized differential quadrature method to structural problems", *Int. J. Numer. Method. Eng.*, **37**(11), 1881-1896. https://doi.org/10.1002/nme.1620371107.

Eltaher, M., Alshorbagy, A. and Mahmoud, F. (2013), "Determination of neutral axis position and its effect on natural frequencies of functionally graded macro/nanobeams", *Compos. Struct.*, **99**, 193-201. https://doi.org/10.1016/j.compstruct.2012.11.039.

Ghorbanpour Arani, A., Kiani, F. and Afshari, H. (2019), "Aeroelastic analysis of laminated FG-CNTRC cylindrical panels under yawed supersonic flow", *Int. J. Appl. Mech.*. **11**(6), 1950052. https://doi.org/10.1142/S1758825119500522.

Ghorbanpour Arani, A., Kiani, F. and Afshari, H. (2019), "Free and forced vibration analysis of laminated functionally graded CNT-reinforced composite cylindrical panels", *J. Sandwich Struct. Mater.*, 1099636219830787.

Grover, N., Singh, B. and Maiti, D. (2016), "An inverse trigonometric shear deformation theory for supersonic flutter characteristics of multilayered composite plates", *Aerospa. Sci. Technol.*, **52**, 41-51. https://doi.org/10.1016/j.ast.2016.02.017.

Haddadpour, H., Mahmoudkhani, S. and Navazi, H. (2008), "Supersonic flutter prediction of functionally graded cylindrical shells", *Compos. Struct.*, **83**(4), 391-398. https://doi.org/10.1016/j.compstruct.2007.05.011.

Han, Y., Liu, S. and Cai, C. (2015), "Flutter stability of a long-span suspension bridge during erection", *Wind Struct.*, **21**(1), 41-61. https://doi.org/10.12989/was.2015.21.1.041.

Hasheminejad, S.M., Nezami, M. and Aryaee Panah, M. (2013), "Flutter suppression of an elastically supported plate with electro-rheological fluid core under yawed supersonic flows", *Int. J. Struct. Stability and Dynamics*. **13**(1), 1250073. https://doi.org/10.1142/S0219455412500733.

Hatami-Marbini, H. and Rohanifar, M. (2019), "Stiffness of bi-modulus hexagonal and diamond honeycombs", *J. Mech. Sci. Technol.*, **33**(4), 1703-1709. https://doi.org/10.1007/s12206-019-0322-1.

Hosseini-Hashemi, S., Fadaee, M. and Atashipour, S.R. (2011), "A new exact analytical approach for free vibration of Reissner–Mindlin functionally graded rectangular plates", *Int. J. Mech. Sci.*, **53**(1), 11-22. https://doi.org/10.1016/j.ijmecsci.2010.10.002.

Hosseini, M. and Fazelzadeh, S. (2010), "Aerothermoelastic post-critical and vibration analysis of temperature-dependent functionally graded panels", *J. Therm. Stresses*, **33**(12), 1188-1212. https://doi.org/10.1080/01495739.2010.510754.

Hosseini, M., Fazelzadeh, S. and Marzocca, P. (2011), "Chaotic and bifurcation dynamic behavior of functionally graded curved panels under aero-thermal loads", *Int. J. Bifurcation Chaos.* **21**(3), 931-954. https://doi.org/10.1142/S0218127411028738.

Kaneko, T. (1975), "On Timoshenko's correction for shear in vibrating beams", *J. Phys. D: Appl. Phys.*, **8**(16), 1927.

Kouchakzadeh, M., Rasekh, M. and Haddadpour, H. (2010), "Panel flutter analysis of general laminated composite plates", *Compos. Struct.*, **92**(12), 2906-2915. https://doi.org/10.1016/j.compstruct.2010.05.001.

Kuo, S.Y. (2011), "Flutter of rectangular composite plates with variable fiber pacing", *Compos. Struct.*, **93**(10), 2533-2540. https://doi.org/10.1016/j.compstruct.2011.04.015.

Mahmoudkhani, S., Haddadpour, H. and Navazi, H. (2010), "Supersonic flutter prediction of functionally graded conical shells", *Compos. Struct.*, **92**(2), 377-386. https://doi.org/10.1016/j.compstruct.2009.08.018.

Meijer, M.C. and Dala, L. (2015), "Zeroth-order flutter prediction for cantilevered plates in supersonic flow", *J. Fluids Struct.*, **57** 196-205. https://doi.org/10.1016/j.jfluidstructs.2015.06.018.

Mindlin, R.D. (1951), "Influence of rotatory inertia and shear on flexural motions of isotropic, elastic plates", *J. Appl. Mech.*, **18** 31.

Navazi, H. and Haddadpour, H. (2011), "Nonlinear aero-thermoelastic analysis of homogeneous and functionally graded plates in supersonic airflow using coupled models", *Compos. Struct.*, **93**(10), 2554-2565. https://doi.org/10.1016/j.compstruct.2011.04.018.

Prakash, T. and Ganapathi, M. (2006), "Supersonic flutter characteristics of functionally graded flat panels including thermal effects", *Compos. Struct.*, **72**(1), 10-18. https://doi.org/10.1016/j.compstruct.2004.10.007.

Sankar, A., Natarajan, S., Zineb, T.B. and Ganapathi, M. (2015), "Investigation of supersonic flutter of thick doubly curved sandwich panels with CNT reinforced facesheets using higher-order structural theory", *Compos. Struct.*, **127**, 340-355. https://doi.org/10.1016/j.compstruct.2015.02.047.

Shin, W.H., Oh, I.K., Han, J.H. and Lee, I. (2006), "Aeroelastic characteristics of cylindrical hybrid composite panels with viscoelastic damping treatments", *J. Sound Vib.*, **296**(1-2), 99-116. https://doi.org/10.1016/j.jsv.2006.01.068.

Singha, M. and Mandal, M. (2008), "Supersonic flutter characteristics of composite cylindrical panels", *Compos. Struct.*, **82**(2), 295-301. https://doi.org/10.1016/j.compstruct.2007.01.007.

Singha, M.K. and Ganapathi, M. (2005), "A parametric study on supersonic flutter behavior of laminated composite skew flat panels", *Compos. Struct.*, **69**(1), 55-63. https://doi.org/10.1016/j.compstruct.2004.04.018.

Srinivasan, R. and Babu, B. (1985), "Flutter analysis of cantilevered quadrilateral plates", *J. Sound Vib.*, **98**(1), 45-53. https://doi.org/10.1016/0022-460X(85)90401-8.

Tang, H., Li, Y., Chen, X., Shum, K.M. and Liao, H. (2017), "Flutter performance of central-slotted plate at large angles of attack", *Wind Struct.*, **24**(5), 447-464. https://doi.org/10.12989/was.2017.24.5.447.

Torabi, K. and Afshari, H. (2016), "Generalized differential quadrature method for vibration analysis of cantilever trapezoidal FG thick plate", *J. Solid Mech.*, **8**(1), 184-203.

Torabi, K. and Afshari, H. (2017), "Optimization for flutter boundaries of cantilevered trapezoidal thick plates", *J. Brazilian Soc. Mech. Sci. Eng.*, **39**(5), 1545-1561.

Torabi, K. and Afshari, H. (2017), "Optimization of flutter boundaries of cantilevered trapezoidal functionally graded sandwich plates", *J. Sandwich Struct. Mater.*, 1099636217697492. https://doi.org/10.1177/1099636217697492.

Torabi, K. and Afshari, H. (2017), "Vibration analysis of a cantilevered trapezoidal moderately thick plate with variable thickness", *Eng. Solid Mech.*, **5**(1), 71-92.

Torabi, K., Afshari, H. and Aboutalebi, F.H. (2017), "Vibration and flutter analyses of cantilever trapezoidal honeycomb sandwich plates", *J. Sandwich Struct. Mater.*, 1099636217728746.

Tounsi, A., Houari, M.S.A., Benyoucef, S. and Adda Bedia, E.A. (2013), "A refined trigonometric shear deformation theory for thermoelastic bending of functionally graded sandwich plates", *Aerosp. Sci. Technol.*, **24**(1), 209-220. https://doi.org/10.1016/j.ast.2011.11.009.

Vedeneev, V.V. (2012), "Panel flutter at low supersonic speeds", *J. Fluid. Struct.*, **29**, 79-96. https://doi.org/10.1016/j.jfluidstructs.2011.12.011.

Vedeneev, V.V. (2013), "Effect of damping on flutter of simply supported and clamped panels at low supersonic speeds", *J. Fluid. Struct.*, **40**, 366-372. https://doi.org/10.1016/j.jfluidstructs.2013.04.004.

Vedeneev, V.V., Guvernyuk, S.V., Zubkov, A.F. and Kolotnikov, M.E. (2010), "Experimental observation of single mode panel flutter in supersonic gas flow", *J. Fluid. Struct.*, **26**(5), 764-779. https://doi.org/10.1016/j.jfluidstructs.2010.04.004.

Wang, K., Liao, H. and Li, M. (2016), "Flutter suppression of long-span suspension bridge with truss girder", *Wind Struct.*, **23**(5), 405-420. https://doi.org/10.12989/was.2016.23.5.405.

CC

Appendix A

Components of matrices [K] and [M] appeared in Eq. (40) are defined as

$$\{s\}=\begin{Bmatrix}\{\bar{U}\}\\ \{\bar{V}\}\\ \{\bar{W}\}\\ \{\bar{X}\}\\ \{\bar{Y}\}\end{Bmatrix}$$

$$[K]=\begin{bmatrix}k_{11} & k_{12} & [0] & k_{14} & k_{15}\\ k_{21} & k_{22} & [0] & k_{24} & k_{25}\\ [0] & [0] & k_{33} & k_{34} & k_{35}\\ k_{41} & k_{42} & k_{43} & k_{44} & k_{45}\\ k_{51} & k_{52} & k_{53} & k_{54} & k_{55}\end{bmatrix} \quad \text{(A-1)}$$

$$[M]=\begin{bmatrix}m_{11} & [0] & [0] & m_{14} & [0]\\ [0] & m_{22} & [0] & [0] & m_{25}\\ [0] & [0] & m_{33} & [0] & [0]\\ m_{41} & [0] & [0] & m_{44} & [0]\\ [0] & m_{52} & [0] & [0] & m_{55}\end{bmatrix}$$

in which [0] is zero matrix of order N*M, $k_{ij}=k_{ji}$, $m_{ij}=m_{ji}$ and

$$k_{11}=\frac{12f_0}{\gamma}\left[I^{(\eta)}\otimes B^{(\zeta)}+\upsilon_1\phi^2\left(B^{(\eta)}\otimes I^{(\zeta)}\right)\right]$$

$$k_{12}=\frac{12\upsilon_2\phi f_0}{\gamma}\left(A^{(\eta)}\otimes A^{(\zeta)}\right)$$

$$k_{14}=3f_1\left[I^{(\eta)}\otimes B^{(\zeta)}+\upsilon_1\phi^2\left(B^{(\eta)}\otimes I^{(\zeta)}\right)\right]$$

$$k_{15}=3\upsilon_2\phi f_1\left(A^{(\eta)}\otimes A^{(\zeta)}\right)$$

$$m_{11}=\gamma\phi^2 g_0\left(I^{(\eta)}\otimes I^{(\zeta)}\right)$$

$$m_{14}=\frac{\gamma^2\phi^2 g_1}{4}\left(I^{(\eta)}\otimes I^{(\zeta)}\right) \quad \text{(A-2)}$$

$$k_{22}=\frac{12f_0}{\gamma}\left[\upsilon_1\left(I^{(\eta)}\otimes B^{(\zeta)}\right)+\phi^2\left(B^{(\eta)}\otimes I^{(\zeta)}\right)\right]$$

$$k_{24}=3\upsilon_2\phi f_1\left(A^{(\eta)}\otimes A^{(\zeta)}\right)$$

$$k_{25}=3f_1\left[\upsilon_1\left(I^{(\eta)}\otimes B^{(\zeta)}\right)+\phi^2\left(B^{(\eta)}\otimes I^{(\zeta)}\right)\right]$$

$$m_{22}=\gamma\phi^2 g_0\left(I^{(\eta)}\otimes I^{(\zeta)}\right)$$

$$m_{25}=\frac{\gamma^2\phi^2 g_1}{4}\left(I^{(\eta)}\otimes I^{(\zeta)}\right)$$

$$k_{33}=-\frac{12k\upsilon_1 f_0}{\gamma}\left[I^{(\eta)}\otimes B^{(\zeta)}+\phi^2\left(B^{(\eta)}\otimes I^{(\zeta)}\right)\right]$$
$$+\frac{\xi_\infty^* m_\infty}{\gamma^2}\left[\phi\cos\theta_\infty\left(I^{(\eta)}\otimes A^{(\zeta)}\right)\right.$$
$$\left.+\phi^2\sin\theta_\infty\left(A^{(\eta)}\otimes I^{(\zeta)}\right)\right]$$

$$k_{34}=-\frac{12k\upsilon_1\phi f_0}{\gamma}\left(I^{(\eta)}\otimes A^{(\zeta)}\right)$$

$$k_{35}=-\frac{12k\upsilon_1\phi^2 f_0}{\gamma}\left(A^{(\eta)}\otimes I^{(\zeta)}\right)$$

$$m_{33}=-\gamma\phi^2 g_0\left(I^{(\eta)}\otimes I^{(\zeta)}\right)$$

$$k_{44}=\gamma f_2\left[I^{(\eta)}\otimes B^{(\zeta)}+\upsilon_1\phi^2\left(B^{(\eta)}\otimes I^{(\zeta)}\right)\right]$$
$$-\frac{12k\upsilon_1\phi^2 f_0}{\gamma}\left(I^{(\eta)}\otimes I^{(\zeta)}\right)$$

$$k_{45}=\upsilon_2\gamma\phi f_2\left(A^{(\eta)}\otimes A^{(\zeta)}\right)$$

$$m_{44}=\frac{\gamma^3\phi^2 g_2}{12}\left(I^{(\eta)}\otimes I^{(\zeta)}\right)$$

$$k_{55}=\gamma f_2\left[\upsilon_1\left(I^{(\eta)}\otimes B^{(\zeta)}\right)+\phi^2\left(B^{(\eta)}\otimes I^{(\zeta)}\right)\right]$$
$$-\frac{12k\upsilon_1\phi^2 f_0}{\gamma}\left(I^{(\eta)}\otimes I^{(\zeta)}\right)$$

$$m_{55}=\frac{\gamma^3\phi^2 g_2}{12}\left(I^{(\eta)}\otimes I^{(\zeta)}\right)$$

Appendix B

Matrix [T] appeared in Eq. (41) is defined as

$$[T]=\begin{bmatrix} T_{11} & T_{12} & T_{13} & T_{14} & T_{15} \\ T_{21} & T_{22} & T_{23} & T_{24} & T_{25} \\ \vdots & \vdots & \vdots & \vdots & \vdots \\ T_{191} & T_{192} & T_{193} & T_{194} & T_{195} \\ T_{201} & T_{202} & T_{203} & T_{204} & T_{205} \end{bmatrix} \tag{B-1}$$

in which

$\eta = 0$:

$$T_{11} = T_{22} = T_{33} = T_{44} = T_{55} = I_{1j}^{(\eta)} \otimes I^{(\zeta)}$$

$$T_{12} = T_{13} = T_{14} = T_{15} = T_{21} = T_{23} = T_{24} = T_{25}$$
$$= T_{31} = T_{32} = T_{34} = T_{35} = T_{41} = T_{42} = T_{43}$$
$$= T_{45} = T_{51} = T_{52} = T_{53} = T_{54} = \{0\}_{N*NM}$$

$\eta = 1$:

$$T_{61} = T_{72} = T_{94} = T_{105} = \phi\left(A_{Mj}^{(\eta)} \otimes I^{(\zeta)}\right)$$

$$T_{62} = T_{95} = I_{Mj}^{(\eta)} \otimes A^{(\zeta)}$$

$$T_{71} = T_{104} = \upsilon\left(I_{Mj}^{(\eta)} \otimes A^{(\zeta)}\right)$$

$$T_{83} = A_{Mj}^{(\eta)} \otimes I^{\zeta}$$

$$T_{85} = I_{Mj}^{(\eta)} \otimes I^{\zeta}$$

$$T_{63} = T_{64} = T_{65} = T_{73} = T_{74} = T_{75} = T_{81} = T_{82} = T_{84}$$
$$= T_{91} = T_{92} = T_{93} = T_{101} = T_{102} = T_{103} = \{0\}_{N*NM}$$

$\zeta = 0$:

$$T_{111} = T_{133} = T_{144} = T_{155} = I^{(\eta)} \otimes A_{1\mathrm{i}}^{(\zeta)}$$

$$T_{112} = T_{145} = \phi\upsilon\left(A^{(\eta)} \otimes I_{1\mathrm{i}}^{(\zeta)}\right)$$

$$T_{121} = T_{154} = \phi\left(A^{(\eta)} \otimes I_{1\mathrm{i}}^{(\zeta)}\right) \tag{B-2}$$

$$T_{122} = I^{(\eta)} \otimes A_{1\mathrm{i}}^{(\zeta)}$$

$$T_{134} = \phi\left(I^{(\eta)} \otimes I_{1\mathrm{i}}^{(\zeta)}\right)$$

$$T_{113} = T_{114} = T_{115} = T_{123} = T_{124} = T_{125}$$
$$= T_{131} = T_{132} = T_{135} = T_{141} = T_{142} = T_{143}$$
$$= T_{151} = T_{152} = T_{153} = \{0\}_{M*NM}$$

$\zeta = 1$:

$$T_{161} = T_{183} = T_{194} = T_{205} = I^{(\eta)} \otimes A_{\mathrm{Ni}}^{(\zeta)}$$

$$T_{162} = T_{195} = \phi\upsilon\left(A^{(\eta)} \otimes I_{\mathrm{Ni}}^{(\zeta)}\right)$$

$$T_{171} = T_{204} = \phi\left(A^{(\eta)} \otimes I_{\mathrm{Ni}}^{(\zeta)}\right)$$

$$T_{172} = I^{(\eta)} \otimes A_{\mathrm{Ni}}^{(\zeta)}$$

$$T_{184} = \phi\left(I^{(\eta)} \otimes I_{\mathrm{Ni}}^{(\zeta)}\right)$$

$$T_{163} = T_{164} = T_{165} = T_{173} = T_{174} = T_{175}$$
$$= T_{181} = T_{182} = T_{185} = T_{191} = T_{192}$$
$$= T_{193} = T_{201} = T_{202} = T_{203} = \{0\}_{M*NM}$$